Geophysical Research Letters

RESEARCH LETTER
10.1029/2021GL093305

Diverse Dynamical Response to Orographic Gravity Wave Drag Hotspots—A Zonal Mean Perspective

P. Sacha[1,2], A. Kuchar[3], R. Eichinger[1,4], P. Pisoft[1], C. Jacobi[3], and H. E. Rieder[2]

[1]Department of Atmospheric Physics, Faculty of Mathematics and Physics, Charles University, Prague, Czech Republic, [2]Institute of Meteorology and Climatology, University of Natural Resources and Life Sciences, Vienna (BOKU), Vienna, Austria, [3]Institute for Meteorology, Universität Leipzig, Leipzig, Germany, [4]Deutsches Zentrum für Luft- und Raumfahrt (DLR), Institut für Physik der Atmosphäre, Oberpfaffenhofen, Germany

Key Points:

- Intermittent parameterized orographic gravity wave drag affects stratospheric large-scale dynamics in a chemistry-climate model
- Dependence of the resolved dynamical response on the hotspot in question underlines the two-way nature of the interaction
- Unsteady nature of the dynamical response sheds new light on how parameterized orographic gravity waves affect stratospheric transport

Supporting Information:

Supporting Information may be found in the online version of this article.

Correspondence to:

P. Sacha,
petr.sacha@boku.ac.at

Citation:

Sacha, P., Kuchar, A., Eichinger, R., Pisoft, P., Jacobi, C., & Rieder, H. E. (2021). Diverse dynamical response to orographic gravity wave drag hotspots—a zonal mean perspective. *Geophysical Research Letters*, *48*, e2021GL093305. https://doi.org/10.1029/2021GL093305

Received 11 MAR 2021
Accepted 29 MAY 2021

Abstract In the extratropical atmosphere, Rossby waves (RWs) and internal gravity waves (GWs) propagating from the troposphere mediate a coupling with the middle atmosphere by influencing the dynamics therein. In state-of-the-art chemistry-climate models (CCMs), RW effects are well resolved while the majority of GW effects have to be parameterized. Here, we analyze orographic GW (OGW) interaction with resolved dynamics in a comprehensive CCM on daily time scales. For this, we apply a recently developed method of strong OGW drag event composites for three pronounced northern hemisphere OGW hotspots. We show that strong OGW drag events are associated with anomalous resolved wave propagation in the stratosphere. Causal links are inferred from previously published work and are supported by the anomalies in zonal circulation and wave activity tendencies. The nature of these anomalies varies depending on the hotspot region, which underlines the parameterized OGW-resolved dynamics interaction being a two-way process.

Plain Language Summary The majority of atmospheric waves are generated near the surface and propagate subsequently upward in the atmosphere. This includes Rossby waves that are resolved in climate models and small-scale gravity waves (GWs) that commonly have to be parameterized. In the middle atmosphere, the waves eventually break, thereby dissipating their momentum and energy, which influences atmospheric dynamics. The interaction of GWs with the large-scale circulation is to date poorly understood. In this study, we associate regionally enhanced GW drag with anomalies in resolved wave propagation in the stratosphere in a comprehensive chemistry-climate model on the time scale of days. For this, we identify strong orographic GW (OGW) events for the three most pronounced northern hemisphere OGW hotspots and construct composites of anomalies of selected variables with respect to the climatological mean. We find that the response of the resolved wavefield strongly depends on the hotspot region, leading to diverse consequences on the large-scale stratospheric circulation. Strong OGW events in the hotspots are in turn determined by the resolved fields from the surface to the level of OGW dissipation, which highlights the two-way coupling between OGWs and resolved flow.

1. Introduction

The Earth's atmosphere is governed by a complex interplay of chemical, physical, and dynamical processes (e.g., Dameris & Loyola, 2011). As part of that interplay, atmospheric waves strongly influence the dynamical state of the atmosphere by transporting momentum and energy, thereby constituting one of the most important coupling mechanisms between atmospheric layers (Yiğit & Medvedev, 2016). In the extratropics, between the upper troposphere—lower stratosphere region and the mesosphere, Rossby waves (RWs) and internal gravity waves (GWs) dominate these processes. In current generation general circulation and chemistry-climate models (CCMs), the majority of the GW spectrum is usually smaller than the model grid resolution and must, therefore, be parameterized (Alexander, 2010; McLandress, 1998). Commonly, two parameterization schemes are employed to distinguish between orographic GWs (OGWs) and non-orographic GWs. GW parameterizations of both types involve various degrees of simplifications for GW sourcing, propagation, and dissipation processes and rely on certain tuneable parameters, which are only poorly constrained by observations (Geller et al., 2013; Plougonven et al., 2020).

Historically, one of the main aims of the OGW parameterizations was to separate the stratospheric polar night jet from the tropospheric subtropical jet by reducing its overall magnitude and increasing easterly wind shear in the upper troposphere (Alexander, 2010; Eichinger et al., 2020; Kim et al., 2003; Miller et al., 1989; Palmer et al., 1986). Since the advent of the so-called wave driving paradigm (Holton et al., 1995) the dynamical effect of OGWs in models has been increasingly evaluated as a contribution to the driving of the advective Brewer-Dobson circulation (BDC; Butchart, 2014; Sato & Hirano, 2019). Another OGW impact that received considerable attention is connected to sudden stratospheric warming (SSW) events (Baldwin et al., 2020), either via the SSW preconditioning and triggering (Albers & Birner, 2014; Richter et al., 2010; Šácha et al., 2016; Samtleben et al., 2019, 2020) or the vortex recovery (Limpasuvan et al., 2012).

Cohen et al. (2013) showed that perturbations to OGW forcing become balanced by changes in resolved wave drag in a mechanistic model, and Cohen et al. (2014) showed further that the response fully develops on a time-scale of days. This compensation mechanism (in fact rather a set of mechanisms; see Cohen et al., 2014) refers to the compensation of the BDC wave driving quantified with the downward control principle (Haynes et al., 1991). It includes RW sourcing by instabilities induced by OGW drag (OGWD) (McLandress & McFarlane, 1993; Sato et al., 2018; Smith, 2003), OGWD impact on RW breaking in the surf zone and the alteration of resolved wave propagation through modification of the background winds (Sigmond & Scinocca, 2010). Further, it has been demonstrated that the OGWD impact on resolved wave fields depends on the spatio-temporal OGWD distribution (Boos & Shaw, 2013; Šácha et al., 2016; Shaw & Boos, 2012) and specifically on the location of OGWD relative to the stationary planetary scale RWs (Samtleben et al., 2019, 2020).

Shepherd (2014) highlighted the interaction between parameterized GWs and the large-scale circulation as one of the most uncertain aspects of climate modeling. However, the compensation mechanism between resolved and unresolved wave drag as a prominent form of the physics-dynamics interaction is to some extent present also in comprehensive CCMs (Eichinger et al., 2020; Kruse, 2020; Sigmond & Shepherd, 2014) and numerical weather prediction models (van Niekerk et al., 2018). On this basis, Sigmond and Shepherd (2014) argued that the existence of the compensation mechanism increases the robustness and confidence in future climate projections, in particular for BDC trends. Recently, in contrast, Eichinger et al. (2020) showed that while the compensation holds to some extent for the advective component of the BDC, the mixing component and thereby the net effect on transport cannot be compensated.

Van Niekerk et al. (2018) documented that the different nature of dynamical impact by parameterized OGWs and resolved OGWs prevents an agreement between high resolution (without OGW parameterization) and low-resolution model versions. This raised the question of how realistic the interaction between OGWD and resolved dynamics is in current CCMs and emphasized the need for further research. A conceptual framework for the research of OGWD impact in CCMs has been outlined in Kruse (2020) by defining relevant time scales for the interaction. On the climatological time scale, this study highlighted that the dominant impact of OGWD are the global scale potential vorticity banners (i.e., elongated filaments of anomalous potential vorticity) leading to anticyclonic anomalies over the polar cap and positive potential vorticity anomalies in the extratropics in the stratosphere. On a time scale of 10 or more days after the OGWD impact, resolved variability dominates, and only on shorter time scales, regional OGWD impacts can be identified.

The aim of the present study is to illustrate how the regionally dependent interaction between intermittent OGWD and resolved dynamics on a short time scale leads to large-scale impacts in the stratosphere. Studying this mechanism is important to pave the way for a full understanding and improvement of troposphere-stratosphere coupling in state-of-the-art CCMs and thereby for advances in the predictability of the coupled atmospheric system. To account for the intermittency of OGWD and its distribution into hotspots, we build on the methodology of strong OGWD composites presented by Kuchar et al. (2020). The underlying method and model data used are briefly described in Section 2. In Section 3, we first study the composite anomalies of the resolved wavefield connected with the strong OGWD hotspot events using the traditional Transformed Eulerian Mean (TEM; Andrews & McIntyre, 1987; Hardiman et al., 2010) framework, discuss the issue of causality and break down the results into composites for the leading zonal wave modes. Subsequently, we describe how the dynamical anomalies are linked with anomalous zonal mean circulation as illustrated by composite anomalies of the zonal mean zonal wind and its tendency. Finally, we highlight the

transient nature of the wavefield response that elucidates why the net OGWD effect on transport cannot be compensated. In the conclusion section, we summarize the key findings of our study and discuss the complexity of the OGWD-resolved wavefield interaction and its relevance for other studies as well as future challenges concerning the OGW impact on the middle atmosphere.

2. Methodology

Following Kuchar et al. (2020), the study is based on data from a simulation for the 1979–2010 period with the Canadian Middle Atmosphere Model (CMAM; McLandress et al., 2013). CMAM is a CCM with 71 levels in the vertical, which extends up to 7×10^{-4} hPa (about 100 km) with variable vertical resolution. It uses a triangular spectral truncation of T47, corresponding to a horizontal resolution of 2.5° × 2.5°, with the physical parameterizations being performed on a 3.75° horizontal grid. On spatial scales of wavenumbers lower than 21, Newtonian relaxation ("nudging") with a 24 h relaxation time-scale is applied toward the 6-hourly horizontal wind and temperature field from ERA-Interim (Dee et al., 2011) up to 1 hPa (see McLandress et al., 2014, for technical details).

OGWD is parameterized using a three-component scheme comprising sourcing and drag associated with freely propagating hydrostatic GWs in the absence of rotation. Moreover, low-level breaking and downslope windstorm flow-associated drag and low-level drag associated with upstream blocking and lee-vortex dynamics are included (Scinocca & McFarlane, 2000). In the present study, we focus on the drag associated with freely propagating OGWs. The scheme employs two vertically propagating zero-phase-speed waves whose direction and magnitude depend on low-level flow and anisotropy of the unresolved topography. For information on tunable parameters of the scheme, the interested reader is referred to McLandress et al. (2013).

Our study is based on strong OGWD event composites of selected variables for the three most prominent northern hemispheric winter OGWD hotspots at 70 hPa, that is, in the valve layer (Kruse et al., 2016), where OGWD is the dominant dynamical forcing in CMAM (see Figure 1 in Kuchar et al., 2020). The selected hotspots are the Rocky Mountains (RM, 235–257.5°E and 27.5–52°N; note that this hotspot was referred to as Western America in Kuchar et al., 2020), the Himalayas (HI, 70–102.5°E and 20–40°N) and Eastern Asia (EA, 110–145°E and 30–48°N). These are computed using the peak-detection algorithm described in Kuchar et al. (2020). This algorithm identifies peaks (local maxima of negative drag) of OGWD that exceed immediate neighbors separated by more than 20 days with amplitudes beyond a normalized threshold. The identification of strong OGWD events allows to calculate composite anomalies of different variables by subtracting daily values from the monthly climatology of SSW-free winters. Composites of variables that are analyzed in this study and all processed data are available via the Mendeley Data repository (Kuchar, 2020).

The response of resolved waves to OGWD is studied using the Eliassen-Palm flux (EPF) diagnostics (Andrews & McIntyre, 1987) and information on wave transience is supplemented by composites of finite-amplitude wave activity tendency ($FAWA_t$; Nakamura & Solomon, 2010). $FAWA_t$ anomalies indicate an unsteady wavefield response due to OGWD influence on the flux of resolved wave activity into the stratosphere (EPF anomalies). $FAWA_t$ and divergence of EPFs are related by the generalized Eliassen-Palm theorem and their sum is conserved for purely linear and conservative waves in the absence of frictional and diabatic effects (Andrews & McIntyre, 1987). The connection of the strong OGWD events with anomalous transience of the wavefield is important for the interpretation of the results presented by Eichinger et al. (2020), which document that a net effect of OGWD on transport cannot be compensated for (see the supporting information to the article for a theoretical explanation).

Due to the methodology applied, our strong OGWD composites also sample specific atmospheric background conditions (wind field, resolved wavefield) that favor strong OGWD events for each hotspot. These conditions can be in general similar for each composited event of the particular hotspot and emerge in our results as significant anomalies, which we refer to as "hotspot preconditioning" further in the text. To distinguish in our results between significant anomalies caused by a causal response to the OGWD and imprints of the "hotspot preconditioning", we rely on the fundamentals of OGW parameterization schemes, knowledge of OGWD dynamical impacts available from the rich body of literature on sensitivity simulations

(Cohen et al., 2013; Eichinger et al., 2020; Šácha et al., 2016; Samtleben et al., 2019, 2020; Sigmond & Scinocca, 2010) and the correspondence between anomalies of different quantities.

3. Results

In this study, we focus on the short-term dynamical response to strong OGWD hotspot events. For this, Figures 1a–1c show the composites of the zonal mean EPFs, their divergence (EPFD), and OGWD anomalies for the three hotspot regions at lag = 0. This corresponds to the peak magnitude of the drag during the respective strong OGWD event. As shown in Figure 8 of Kuchar et al. (2020), the peak is already preceeded by a few days of significant OGWD anomalies in the region of the hotspot. Therefore, at lag = 0 we can see a response that has already been evolving over a few days prior to lag = 0 under an increasing OGWD forcing overlapping with an imprint of the "hotspot preconditioning." To assess if nudging has a dynamical impact on the composites, we derived the nudging strength as a residual term from the TEM momentum budget (see Equation S1). Except locally in the polar mesosphere, the nudging strength composites (Figure S1 in the Supplement) are largely not significant and generally smaller than the EPFD or OGWD anomalies allowing us to neglect the nudging effects on the presented results.

Figures 1a–1c show negative zonal mean OGWD anomalies (stronger drag) corresponding to the location of the hotspots at around 70 hPa (green lines). Moreover, strong OGWD events in the hotspots are connected with zonal mean OGWD anomalies in the upper stratosphere and mesosphere (see Kuchar et al., 2020 for more details), which are mainly positive. The composite for the RM hotspot reveals a positive OGWD anomaly in the lower stratosphere poleward from 60°N. This anomaly is connected with the lack of negative OGWD northward from the RM hotspot together with the orography around the Northern Pacific, which acts as a source of positive OGWD in the lower stratosphere during periods favorable for strong OGWD events in the RM hotspot (the interested reader is referred to Figure S2 in the Supplement showing anomalies in the surface wind stress).

Studies with comprehensive climate models have shown that the dominant response to OGW perturbations in the winter stratosphere is the modulation of refractive properties and subsequent changes in the propagation of resolved waves (Eichinger et al., 2020; Sigmond & Scinocca, 2010; Sigmond & Shepherd, 2014). Climatologically, the resolved waves propagate from the extratropical troposphere upward and equatorward in the stratosphere. As a response to increased OGWD, the equatorward component of the propagation is suppressed and an enhanced fraction of resolved waves is deflected to the stratospheric high latitudes. Our results (Figures 1a–1c) illustrate that a common feature for all hotspots is the alteration of resolved wave propagation in the stratosphere, however the effect differs between the hotspots.

For the HI hotspot, which is the southernmost of the three hotspots, resolved wave propagation is enhanced in the lower stratosphere (denoted by the equatorward and upward-pointing EPF anomalies in the extratropics). However, above approximately 20 km, the waves are reflected poleward, resulting in a negative EPFD anomaly in the stratosphere between 60 and 80°N. For the EA hotspot, resolved wave propagation is suppressed, resulting in patchy positive EPFD anomalies above the hotspot. For the RM hotspot, a suppressed upward propagation of resolved waves throughout the stratosphere leads to significant positive EPFD anomalies, but only near the stratopause (and continuing to the mesosphere, see Figures S3a–S3c). The diversity of the resolved wave anomalies in the stratosphere dependent on the hotspot is in agreement with mechanistic model studies with artificial OGWD enhancements (see Šácha et al., 2016 for the EA hotspot and Samtleben et al., 2019, 2020 also for different regions). This indicates that the anomalous resolved wave propagation starting from the lower stratosphere is directly caused by the strong OGWD events and not by the "hotspot preconditioning".

Locally significant anomalies in the resolved wavefield can be found in the vicinity of the tropopause and in the lower stratosphere below the hotspots as well. These anomalies provide a basis for the direct modulation by OGWD higher in the stratosphere, however, their causality remains elusive and requires further research. According to Sigmond and Shepherd (2014) a direct effect of OGWD cannot be excluded, as the OGWD modification of lower stratospheric winds has been shown to modify also the critical lines for resolved waves below this region. On the other side, we can find pronounced significant EPFD anomalies

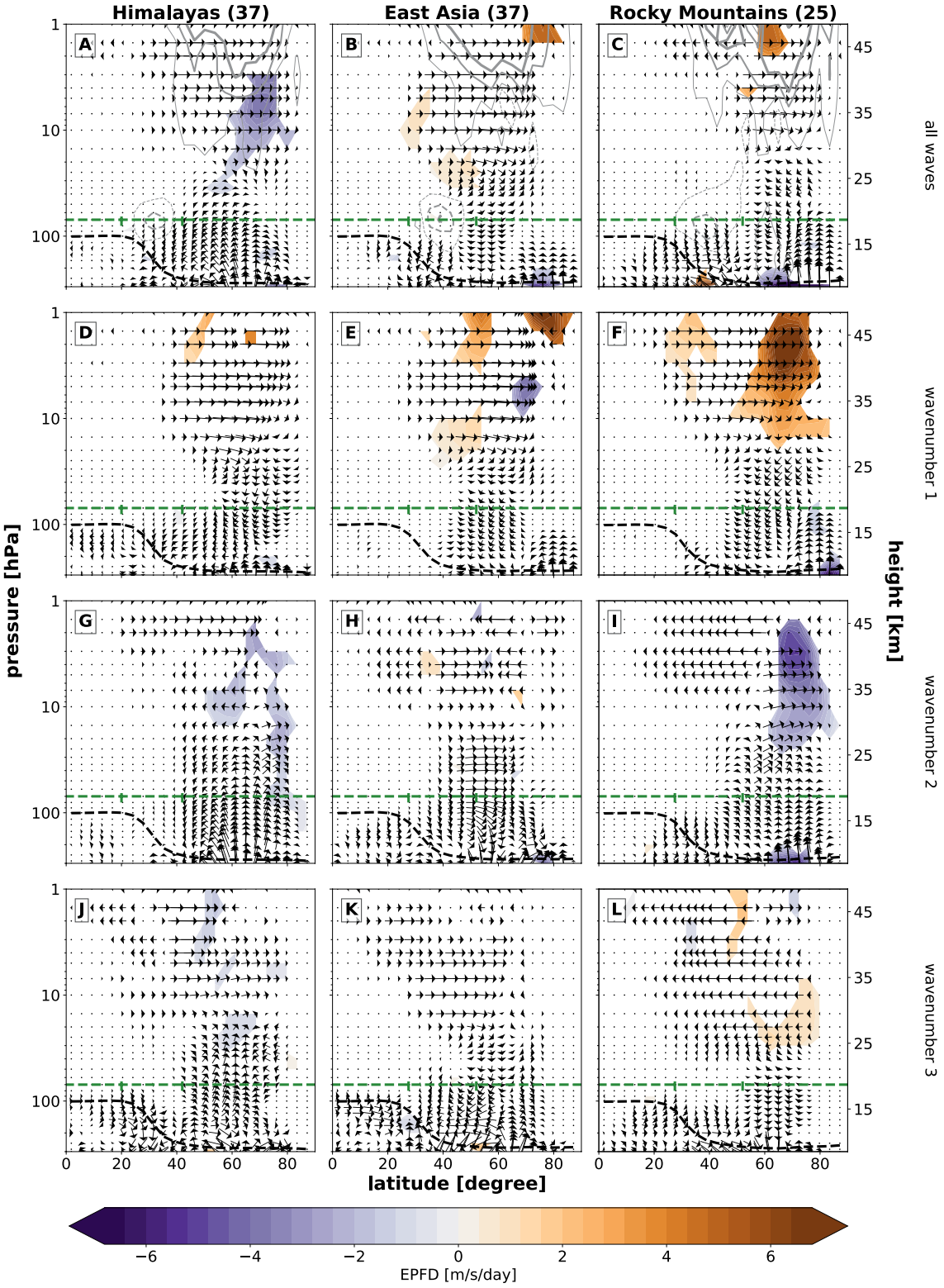
Himalayas (37)
East Asia (37)
Rocky Mountains (25)
A
B
C
D
E
F
G
H
I
J
K
L
all waves
wavenumber 1
wavenumber 2
wavenumber 3
pressure [hPa]
height [km]
latitude [degree]
EPFD [m/s/day]

Figure 1

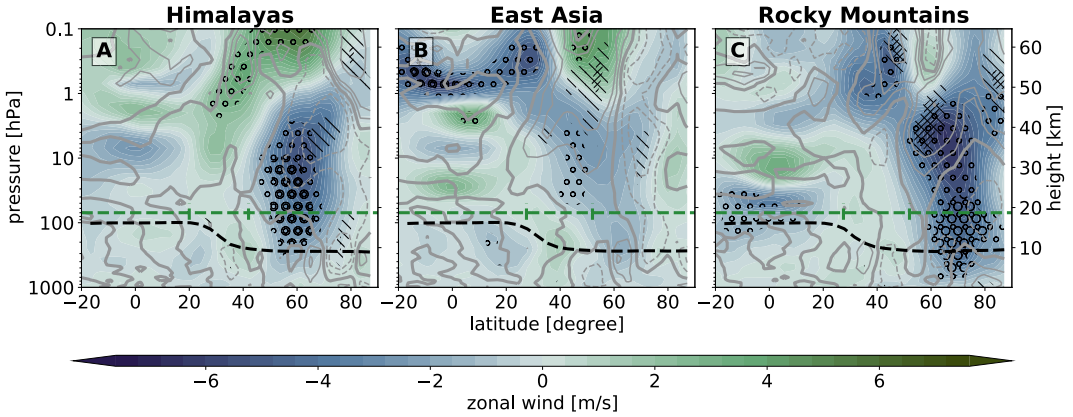

Figure 2. Composite anomalies of zonal mean zonal wind (shading; units: m/s) and its tendency (gray contour levels: **0**, ±0.5, ±1, ±3 m/s/day) at lag = 0 representing the Himalaya (left panel), East Asia (middle panel) and the Rocky Mountains (right panel) hotspot composites. The tropopause and hotspot locations are plotted as in Figure 1. Circles oooo and 𝕆𝕆𝕆𝕆 show where the *p*-values of the zonal-wind anomalies are <0.05 and <0.01, respectively. Hatching \\\\ and //// shows where the *p*-values of the zonal-wind tendency anomalies are <0.05 and <0.01, respectively.

starting already in the lower troposphere for all hotspots (Figures S3g–S3i) that can clearly be attributed to the preconditioning of the strong OGWD events for each hotspot.

Samtleben et al. (2020) have shown that the OGWD influence on the zonal mean dynamics is mainly driven by changes in the propagation of planetary-scale RWs with zonal wavenumber 1 (PW1). Decomposition of the EPF and EPFD anomalies according to the wavenumber (Figures 1d–1l) shows that the propagation of PW1 is suppressed for all three hotspots. In contrast, Samtleben et al. (2020) only report a suppression for the EA and HI hotspots. This discrepancy can be explained by the fact that the results of Samtleben et al. (2020) are valid only for one selected climatological background state (including the relative position of the hotspots to the surf zone extent) and a stationary PW phase setup. For instance, the geographical location of the EA hotspot is exactly such that the stratospheric response is out of phase with the climatological stationary PW1 in Samtleben et al. (2020). In the present study, however, the "hotspot preconditioning" has to be considered as well, indicating that the background PW field differs for each hotspot and also from the background situation in Samtleben et al. (2020).

Decomposing the net EPF anomalies into different PW modes reveals that the net (mostly insignificant) EPFD anomaly for the RM hotspot masks strong PW1 suppression and strongly enhanced propagation and anomalous dissipation of PW2 in the polar vortex region. For the HI hotspot, the net anomalous EPF convergence in the vortex region is caused by enhanced PW2 and PW3 propagation toward the vortex. This results in stronger dissipation in a broad vertical region of the stratosphere. EPF composites for higher wavenumber PWs are mostly insignificant (not shown).

The strong OGWD events for the HI and RM hotspots are connected with significant anomalies of the zonal mean circulation, see the zonal mean zonal wind composites in Figure 2. The most pronounced anomalies are the weakened zonal winds in the stratospheric polar vortex region, where the signal is significant across the entire stratosphere. For HI this is followed above 1 hPa with stronger zonal winds in the region of the polar night jet. To determine if the anomalies are connected with the "hotspot preconditioning", or whether some aspects of the anomalies are a direct effect of the strong OGWD events, we show in Figure 2 the zonal mean zonal wind tendency anomalies (contours). For the HI hotspot, the anomalous negative wind tendency supports the zonal mean zonal wind anomaly in the polar vortex, which is well collocated with

Figure 1. Composite anomalies of Eliassen-Palm flux $\vec{F}$ (arrows; units: [1; 10^{-2}] kg/s/s) and its divergence $\nabla \cdot \vec{F}$ (shading; units: m/s/day) and zonal mean orographic gravity wave drag anomalies (gray solid (positive) and dashed (negative) contours: ±0.1, ±0.5, ±1, ±3 m/s/day, linewidths increase with increasing values) at lag = 0 for the Himalayas (left panels), East Asia (middle panels) and the Rocky Mountains (right panels). In panels (d–l) the anomalies are decomposed into leading zonal planetary wave modes. The values in brackets at the top of the panels indicate the total number of composited events for each hotspot. The green horizontal and vertical lines represent regions of the particular gravity wave hotspot and the 70 hPa level. The black dashed line denotes tropopause pressure of the respective composite. The Eliassen-Palm flux divergence anomalies are colored only where the p-values of the anomalies are <0.05.

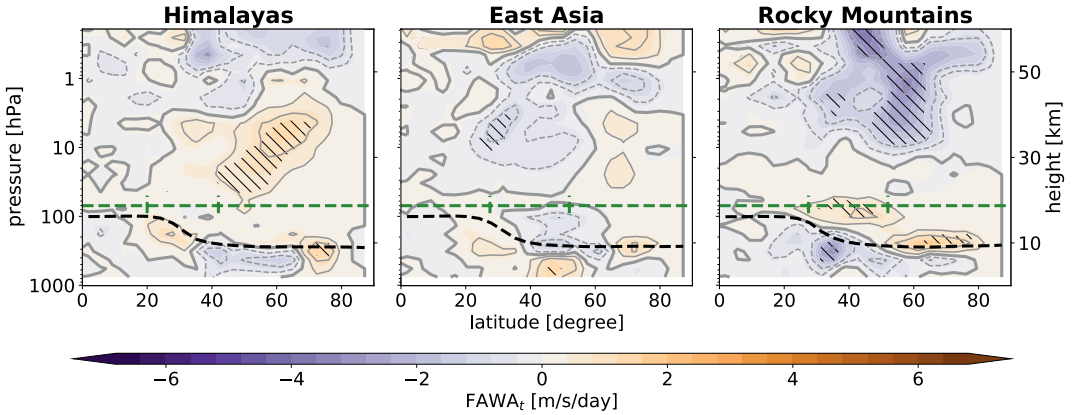

Figure 3. Zonal mean finite-amplitude wave activity tendency (FAWA$_t$; shading; units: m/s/day) and absolute average (gray contour levels: **0**, ±0.5, ±1, ±3 m/s/day) composite averages at lag = 0 representing the Himalayas (left panel), East Asia (middle panel) and the Rocky Mountains (right panel). The tropopause, hotspot locations and statistical significance are plotted as in Figure 1. Hatching \\\\ and //// shows where the p-values of the anomalies are <0.05 and <0.01, respectively.

the region of enhanced dissipation of resolved waves. This together indicates that for HI the strong OGWD events support the polar vortex deceleration. For the RM hotspot, the anomalous zonal mean zonal wind tendency supports the polar vortex deceleration only in the lower stratosphere to some degree, higher above the sign is reversed. Moreover, the opposing sign of EPFD anomalies of leading PW modes for RM, does not allow us to cleanly determine the causality of the zonal mean circulation anomalies for this hotspot.

A rich body of literature details a link between anomalous resolved wave activity and SSWs (see e.g., Hoffmann et al., 2007; Labitzke, 1977; Schoeberl, 1978), which suggests a possible role of the strong OGWD events for SSWs, particularly for HI. In our analysis, the polar vortex anomaly is found to be especially strong when the HI composites are additionally filtered according to the quasi-biennial oscillation phase (see Figure S4). This suggests that the HI hotspot may play a role in the Holton-Tan mechanism (Garfinkel et al., 2012), however, longer time series are required to constitute conclusive and statistically robust results in this respect.

For the EA hotspot, Figure 2 shows a negative zonal wind anomaly above the hotspot up to about 40 km that reverses into a positive anomaly above around 50 km. The negative anomaly above the hotspot is in line with findings of Pisoft et al. (2018), who showed that the EA hotspot is connected with the local occurence of a critical layer for the GW propagation. Another preconditioning feature of the EA hotspot is the statistically significant zonal wind anomalies in the equatorial region. This indicates that the strong OGWD events in the EA hotspot are sensitive to the quasi-biennial oscillation phase, a result in agreement with the findings of Šácha et al. (2018) (see their Figure 3). Note that for the EA hotspot no significant zonal wind anomalies (from the SSW-free climatology) emerge in the polar vortex region. In line with the OGWD induced suppression of the resolved wave propagation, the zonal mean zonal wind tendency anomalies are positive, in contrast to the negative wind anomaly above the hotspot, and accelerating the polar vortex around 60°N. This is an important finding in the context of the results of White et al. (2018). Following the results of model experiments with flattened Mongolian topography, these authors found a substantial decrease in the occurrence frequency of SSWs, and argued for the uttermost importance of the Mongolian topography for the stratospheric winter circulation. However, their Figure S4 shows that the orography modifications also result in enhanced zonal mean OGWD in midlatitudes, likely including strong OGWD enhancement in the EA hotspot (which is located directly downwind), which consequently prevents deceleration of the stratospheric polar vortex by resolved waves as described above.

The composite analysis of strong OGWD events allows us to study the short-term, unsteady response to OGWD. It is therefore natural to expect that also the resolved wavefield response studied in Figure 1 will have an unsteady component. For this, we show FAWA$_t$ anomalies in Figure 3 that illustrate the tendency of the resolved wave activity measured by changes of their amplitudes (i.e., wave transience). The EA hotspot

shows negative $FAWA_t$ anomalies corresponding to the positive EPFD anomalies in Figure 1b. This collocation documents the overall suppression of wave activity above and equatorward from the hotspot due to suppressed propagation of resolved waves by strong OGWD events in this hotspot. The HI hotspot induces increasing wave activity in the stratosphere from middle to polar latitudes and also locally around the polar tropopause in accordance with the negative EPFD anomalies resulting from the enhanced resolved wave propagation due to the strong OGWD events. For RM, we find multiple regions with significant $FAWA_t$ anomalies, both positive and negative (a large region in the upper stratosphere and mesosphere). The anomalies are not well collocated with the EPFD anomalies, which points to the role of frictional (OGWD) or possibly diabatic processes influencing the wave activity during the RM strong OGWD events. Of particular note is the positive $FAWA_t$ anomaly inside the latitudinal band of the hotspot, which suggests that the OGWD may function as an in-situ source of resolved wave activity in the RM hotspot. Altogether, the causality of $FAWA_t$ anomalies (and also of the zonal mean zonal wind and EPFD anomalies) for the RM hotspot cannot be inferred in the zonal mean framework. This issue demands a dedicated follow-up study of the dynamical mechanisms at a regional scale.

In general, the occurrence of $FAWA_t$ anomalies can explain why the OGWD impact on stratospheric transport cannot generally be compensated in CCMs (Eichinger et al., 2020). The transient nature of the resolved wavefield response to intermittent OGWD in the stratosphere deteriorates the approximation of the advective transport by the residual mean circulation, which is then attributed as a change in mixing strength.

4. Conclusions

In this study, we analyze the impact of parameterized OGWD from the three dominant NH hotspots on stratospheric dynamics, fully respecting the intermittency of OGWD in a CCM. This is achieved by building on the methodology of strong OGWD event composites developed by Kuchar et al. (2020). Within days, strong OGWD events significantly affect large-scale stratospheric dynamics mainly by altering the propagation of the first three dominant zonal PW modes. Our results demonstrate that the influence of the strong OGWD events on resolved dynamics depends on the region of forcing and on the background conditions favorable for the strong OGWD event in the hotspot. In particular, suppression of resolved wave propagation in the stratosphere dominates for the EA hotspot, while deflection and stronger wave propagation toward the stratospheric polar vortex is dominant for the HI hotspot. For the RM hotspot, a combination of both effects emerges, in magnitude and effect depending on the PW mode. The alteration of large-scale dynamics is connected with significant zonal mean circulation anomalies as demonstrated for zonal mean zonal wind and its tendency. For the HI hotspot, the polar vortex is significantly decelerated and the OGWD effect supports further deceleration. The RM hotspot is connected with a negative polar vortex anomaly as well, but with the attribution of the underlying cause left for further research. In contrast to the latter two hotspots, strong OGWD events in the EA hotspot are not connected with significant polar vortex anomalies and the OGWD impact supports a strengthening of the polar vortex around 60°N. Strong OGWD events also affect the transience of the resolved wavefield in the stratosphere, by controlling the influx of resolved wave activity from below. This leads to a negative wave activity tendency anomaly for EA and RM and to a positive anomaly in the case of HI. This is an important aspect for research of OGWD impact on stratospheric transport.

Our findings demonstrate the complexity of interaction between resolved wave drag and parameterized OGWD in CCMs. The OGWD impact on resolved dynamics strongly depends on the hotspot in play, and strong OGWD events in a hotspot, in turn, depend on tropospheric and stratospheric conditions favorable for the occurrence of the strong OGWD event in the hotspot. We term these background conditions a "hotspot preconditioning" throughout the manuscript. It also includes the impact of resolved wave fields on OGW propagation and breaking within the parameterization (e.g., the EA hotspot dependence on the critical level occurrence), which adds a considerable portion of nonlinearity to the interaction. This suggests that the compensation between resolved and unresolved wave forcing in CCMs is an even more general (and two-way) mechanism than described in Cohen et al. (2014). This complexity implies the futility of modified regional orography model experiments, where the resolved wave versus OGW causal effects cannot be separated.

Furthermore, as OGWD affects not only resolved wave drag in a stationary limit, but also resolved wave activity and transience with direct links to stratospheric variability and transport, it reinforces the importance of OGWD for SSW and stratospheric transport studies. We illustrated how the parameterized OGWD with its non-homogeneous distribution and intermittency acts as a quick communicator in troposphere-stratosphere coupling in this CCM simulation, however, future research will have to evaluate how realistic this process is. In that respect, it will be crucial to study whether the efficient interaction between OGWD and leading PWs appears also for more realistic OGW parameterizations (e.g., including oblique propagation or unsteady schemes) or in simulations of high-resolution models where the majority of the GW spectrum can be resolved.

Data Availability Statement

All processed data files for this study are provided via Mendeley Data Kuchar (2020), and all codes to reproduce our figures are provided via GitHub (Kuchar, 2021).

Acknowledgments
PS is supported through the project CZ.02.2.69/0.0/0.0/19_074/0016231 (International mobility of researchers at Charles University MSCA-IF III) for the research stay at BOKU Vienna. AK and CJ acknowledge support from Deutsche Forschungsgemeinschaft under grant JA836/43-1 (VACILT). RE was funded by the Helmholtz Association under grant VH-NG-1014 (Helmholtz-Hochschul-Nachwuchsforschergruppe MAC-Clim). P Pisoft and R Eichinger are supported by GA CR under Grant Nos. 21-20293J and 21-03295S. Further, PS would like to acknowledge discussions with Rachel White and with members of the New Quantitative Constraints on Orographic Gravity Wave Stress and Drag Satisfying Emerging Needs in Seasonal-to-Subseasonal and Climate Prediction team at the ISSI Bern. The authors would like to thank all colleagues involved in the CMAM-sd model simulation (obtained from http://climate-modelling.canada.ca/climatemodeldata/cmam/output/CMAM/CMAM30-SD/index.shtml, last access: 25 September 2020). Furthermore, we acknowledge developers of python open-source software libraries used for this paper: *aostools* (Jucker, 2018), *cartopy* (Met Office, 2010–2015), *matplotlib* (Hunter, 2007), *numpy* (Oliphant, 2006), *pandas* (McKinney, 2010), *seaborn* (Waskom et al., 2016), *scipy* (Virtanen et al., 2020), *xarray* (Hoyer et al., 2016), and Scientific color maps (Crameri, 2020).

References

Albers, J. R., & Birner, T. (2014). Vortex preconditioning due to planetary and gravity waves prior to sudden stratospheric warmings. *Journal of the Atmospheric Sciences*, *71*(11), 4028–4054. https://doi.org/10.1175/JAS-D-14-0026.1

Alexander, M. J. (2010). Gravity waves in the stratosphere. In *The stratosphere: Dynamics, transport, and chemistry* (pp. 109–121). American Geophysical Union. https://doi.org/10.1029/2009GM000864

Andrews, D. G., & McIntyre, M. E. (1987). *JR Holton, and CB Leovy, 1987: Middle atmosphere dynamics*. Academic Press.

Baldwin, M. P., Ayarzagüena, B., Birner, T., Butchart, N., Charlton-Perez, A. J., Butler, A. H., et al. (2020). Sudden stratospheric warmings. *Earth and Space Science Open Archive*, *49*. https://doi.org/10.1002/essoar.10502884.1

Boos, W. R., & Shaw, T. A. (2013). The effect of moist convection on the tropospheric response to tropical and subtropical zonally asymmetric torques. *Journal of the Atmospheric Sciences*, *70*(12), 4089–4111. https://doi.org/10.1175/JAS-D-13-041.1

Butchart, N. (2014). The Brewer-Dobson circulation. *Reviews of Geophysics*, *52*(2), 157–184. https://doi.org/10.1002/2013RG000448

Cohen, N. Y., Gerber, E. P., & Bühler, O. (2013). Compensation between resolved and unresolved wave driving in the stratosphere: Implications for downward control. *Journal of the Atmospheric Sciences*, *70*(12), 3780–3798. https://doi.org/10.1175/JAS-D-12-0346.1

Cohen, N. Y., Gerber, E. P., & Bühler, O. (2014). What drives the Brewer-Dobson circulation? *Journal of the Atmospheric Sciences*, *71*(10), 3837–3855. https://doi.org/10.1175/JAS-D-14-0021.1

Crameri, F. (2020). *Scientific color maps* (The development of the scientific color maps is supported by the Research Council of Norway through its Centers of Excellence funding scheme, Project Number 223272). Zenodo. https://doi.org/10.5281/zenodo.4153113

Dameris, M., & Loyola, D. (2011). Chemistry-climate connections–interaction of physical, dynamical, and chemical processes in earth atmosphere. In Climate change-geophysical foundations and ecological effects. InTech.

Dee, D. P., Uppala, S. M., Simmons, A. J., Berrisford, P., Poli, P., Kobayashi, S., et al. (2011). The ERA-Interim reanalysis: Configuration and performance of the data assimilation system. *Quarterly Journal of the Royal Meteorological Society*, *137*(656), 553–597. https://doi.org/10.1002/qj.828

Eichinger, R., Garny, H., Šácha, P., Danker, J., Dietmüller, S., & Oberländer-Hayn, S. (2020). Effects of missing gravity waves on stratospheric dynamics; part 1: Climatology. *Climate Dynamics*, *54*(5), 3165–3183.

Garfinkel, C. I., Shaw, T. A., Hartmann, D. L., & Waugh, D. W. (2012). Does the Holton-Tan mechanism explain how the quasi-biennial oscillation modulates the arctic polar vortex? *Journal of the Atmospheric Sciences*, *69*(5), 1713–1733. Retrieved from https://doi.org/10.1175/JAS-D-11-0209.1

Geller, M. A., Alexander, M. J., Love, P. T., Bacmeister, J., Ern, M., Hertzog, A., et al. (2013). A comparison between gravity wave momentum fluxes in observations and climate models. *Journal of Climate*, *26*(17), 6383–6405. https://doi.org/10.1175/JCLI-D-12-00545.1

Hardiman, S. C., Andrews, D. G., White, A. A., Butchart, N., & Edmond, I. (2010). Using different formulations of the transformed Eulerian mean equations and Eliassen-Palm diagnostics in general circulation models. *Journal of the Atmospheric Sciences*, *67*(6), 1983–1995. https://doi.org/10.1175/2010JAS3355.1

Haynes, P. H., McIntyre, M. E., Shepherd, T. G., Marks, C. J., & Shine, K. P. (1991). On the "downward control" of extratropical diabatic circulations by Eddy-induced mean zonal forces. *Journal of the Atmospheric Sciences*, *48*(4), 651–678. Retrieved from https://doi.org/10.1175/1520-0469(1991)048<0651:OTCOED>2.0.CO;2

Hoffmann, P., Singer, W., Keuer, D., Hocking, W., Kunze, M., & Murayama, Y. (2007). Latitudinal and longitudinal variability of mesospheric winds and temperatures during stratospheric warming events. *Journal of Atmospheric and Solar-Terrestrial Physics*, *69*(17), 2355–2366. (Vertical Coupling in the Atmosphere/Ionosphere System). https://doi.org/10.1016/j.jastp.2007.06.010

Holton, J. R., Haynes, P. H., McIntyre, M. E., Douglass, A. R., Rood, R. B., & Pfister, L. (1995). Stratosphere-troposphere exchange. *Reviews of Geophysics*, *33*(4), 403–439. https://doi.org/10.1029/95RG02097

Hoyer, S., Fitzgerald, C., Hamman, J., akleeman Kluyver, T., Roos, M., Hilboll, A, et al. (2016). *xarray: v0.8.0*. https://doi.org/10.5281/zenodo.59499

Hunter, J. D. (2007). Matplotlib: A 2d graphics environment. *Computing in Science & Engineering*, *9*(3), 90–95.

Jucker, M. (2018). *mjucker/aostools: aostools v2.1.5*. Zenodo. https://doi.org/10.5281/zenodo.1252733

Kim, Y.-J., Eckermann, S. D., & Chun, H.-Y. (2003). An overview of the past, present and future of gravity wave drag parametrization for numerical climate and weather prediction models. *Atmosphere-Ocean*, *41*(1), 65–98. https://doi.org/10.3137/ao.410105

Kruse, C. G. (2020). Regional to global evolution of impacts of parameterized mountain-wave drag in the lower stratosphere. *Journal of Climate*, *33*(8), 3093–3106. https://doi.org/10.1175/JCLI-D-19-0076.1

Kruse, C. G., Smith, R. B., & Eckermann, S. D. (2016). The midlatitude lower-stratospheric mountain wave "valve layer". *Journal of the Atmospheric Sciences*, *73*(12), 5081–5100. https://doi.org/10.1175/JAS-D-16-0173.1

Kuchar, A. (2020). *Accompanying data to "On the intermittency of orographic gravity wave hotspots and its importance for middle atmosphere dynamics"*. Mendeley Data. https://doi.org/10.17632/j3hj7f9t67.3
Kuchar, A. (2021). *kuchaale/grl_2020: First release of my GRL2020 code repository*. Zenodo. https://doi.org/10.5281/zenodo.4740482
Kuchar, A., Sacha, P., Eichinger, R., Jacobi, C., Pisoft, P., & Rieder, H. E. (2020). On the intermittency of orographic gravity wave hotspots and its importance for middle atmosphere dynamics. *Weather and Climate Dynamics*, *1*(2), 481–495. https://doi.org/10.5194/wcd-1-481-2020
Labitzke, K. (1977). Interannual variability of the winter stratosphere in the Northern Hemisphere. *Monthly Weather Review*, *105*(6), 762–770. https://doi.org/10.1175/1520-0493(1977)105<0762:IVOTWS>2.0.CO;2
Limpasuvan, V., Richter, J. H., Orsolini, Y. J., Stordal, F., & Kvissel, O.-K. (2012). The roles of planetary and gravity waves during a major stratospheric sudden warming as characterized in WACCM. *Journal of Atmospheric and Solar-Terrestrial Physics*, *78–79*, 84–98. https://doi.org/10.1016/j.jastp.2011.03.004
McKinney, W. (2010). Data structures for statistical computing in python. In S. van der Walt, & J. Millman (Eds.), *Proceedings of the 9th Python in Science Conference* (pp. 51–56).
McLandress, C. (1998). On the importance of gravity waves in the middle atmosphere and their parameterization in general circulation models. *Journal of Atmospheric and Solar-Terrestrial Physics*, *60*(14), 1357–1383.
McLandress, C., & McFarlane, N. (1993). Interactions between orographic gravity wave drag and forced stationary planetary waves in the winter northern hemisphere middle atmosphere. *Journal of the Atmospheric Sciences*, *50*(13), 1966–1990.
McLandress, C., Plummer, D. A., & Shepherd, T. G. (2014). Technical note: A simple procedure for removing temporal discontinuities in era-interim upper stratospheric temperatures for use in nudged chemistry-climate model simulations. *Atmospheric Chemistry and Physics*, *14*(3), 1547–1555. https://doi.org/10.5194/acp-14-1547-2014
McLandress, C., Scinocca, J. F., Shepherd, T. G., Reader, M. C., & Manney, G. L. (2013). Dynamical control of the mesosphere by orographic and nonorographic gravity wave drag during the extended Northern Winters of 2006 and 2009. *Journal of the Atmospheric Sciences*, *70*(7), 2152–2169. https://doi.org/10.1175/JAS-D-12-0297.1
Met Office. (2010–2015). *Cartopy: A cartographic python library with a matplotlib interface* [Computer software manual]. Retrieved from http://scitools.org.uk/cartopy
Miller, M. J., Palmer, T. N., & Swinbank, R. (1989). Parametrization and influence of subgridscale orography in general circulation and numerical weather prediction models. *Meteorology and Atmospheric Physics*, *40*(1), 84–109. https://doi.org/10.1007/BF01027469
Nakamura, N., & Solomon, A. (2010). Finite-amplitude wave activity and mean flow adjustments in the atmospheric general circulation. Part I: Quasigeostrophic theory and analysis. *Journal of the Atmospheric Sciences*, *67*(12), 3967–3983. https://doi.org/10.1175/2010JAS3503.1
Niekerk, van, A., Sandu, I., & Vosper, S. B. (2018). The circulation response to resolved versus parametrized orographic drag over complex mountain terrains. *Journal of Advances in Modeling Earth Systems*, *10*(10), 2527–2547. https://doi.org/10.1029/2018MS001417
Oliphant, T. E. (2006). *A guide to numpy* (Vol. 1). Trelgol Publishing USA.
Palmer, T. N., Shutts, G. J., & Swinbank, R. (1986). Alleviation of a systematic westerly bias in general circulation and numerical weather prediction models through an orographic gravity wave drag parametrization. *Quarterly Journal of the Royal Meteorological Society*, *112*(474), 1001–1039. https://doi.org/10.1002/qj.49711247406
Pisoft, P., Sacha, P., Miksovsky, J., Huszar, P., Scherllin-Pirscher, B., & Foelsche, U. (2018). Revisiting internal gravity waves analysis using GPS RO density profiles: Comparison with temperature profiles and application for wave field stability study. *Atmospheric Measurement Techniques*, *11*(1), 515–527. https://doi.org/10.5194/amt-11-515-2018
Plougonven, R., de la Cámara, A., Hertzog, A., & Lott, F. (2020). How does knowledge of atmospheric gravity waves guide their parameterizations? *Quarterly Journal of the Royal Meteorological Society*, *146*(728), 1529–1543. https://doi.org/10.1002/qj.3732
Richter, J. H., Sassi, F., & Garcia, R. R. (2010). Toward a physically based gravity wave source parameterization in a general circulation model. *Journal of the Atmospheric Sciences*, *67*(1), 136–156. https://doi.org/10.1175/2009JAS3112.1
Šácha, P., Lilienthal, F., Jacobi, C., & Pišoft, P. (2016). Influence of the spatial distribution of gravity wave activity on the middle atmospheric dynamics. *Atmospheric Chemistry and Physics*, *16*(24), 15755–15775. https://doi.org/10.5194/acp-16-15755-2016
Šácha, P., Miksovsky, J., & Pisoft, P. (2018). Interannual variability in the gravity wave drag—Vertical coupling and possible climate links. *Earth System Dynamics*, *9*(2), 647–661. https://doi.org/10.5194/esd-9-647-2018
Samtleben, N., Jacobi, C., Pišoft, P., Šácha, P., & Kuchař, A. (2019). Effect of latitudinally displaced gravity wave forcing in the lower stratosphere on the polar vortex stability. *Annales Geophysicae Discussions*, *2019*, 1–21. https://doi.org/10.5194/angeo-2019-15
Samtleben, N., Kuchař, A., Šácha, P., Pišoft, P., & Jacobi, C. (2020). Impact of local gravity wave forcing in the lower stratosphere on the polar vortex stability: Effect of longitudinal displacement. *Annales Geophysicae*, *38*(1), 95–108. https://doi.org/10.5194/angeo-38-95-2020
Sato, K., & Hirano, S. (2019). The climatology of the brewer–dobson circulation and the contribution of gravity waves. *Atmospheric Chemistry and Physics*, *19*(7), 4517–4539. https://doi.org/10.5194/acp-19-4517-2019
Sato, K., Yasui, R., & Miyoshi, Y. (2018). The momentum budget in the stratosphere, mesosphere, and lower thermosphere. Part I: Contributions of different wave types and in situ generation of Rossby waves. *Journal of the Atmospheric Sciences*, *75*(10), 3613–3633. https://doi.org/10.1175/JAS-D-17-0336.1
Schoeberl, M. R. (1978). Stratospheric warmings: Observations and theory. *Reviews of Geophysics*, *16*(4), 521–538. https://doi.org/10.1029/RG016i004p00521
Scinocca, J. F., & McFarlane, N. A. (2000). The parametrization of drag induced by stratified flow over anisotropic orography. *Quarterly Journal of the Royal Meteorological Society*, *126*(568), 2353–2393. https://doi.org/10.1002/qj.49712656802
Shaw, T. A., & Boos, W. R. (2012). The tropospheric response to tropical and subtropical zonally asymmetric torques: Analytical and idealized numerical model results. *Journal of the Atmospheric Sciences*, *69*(1), 214–235. https://doi.org/10.1175/JAS-D-11-0139.1
Shepherd, T. G. (2014). Atmospheric circulation as a source of uncertainty in climate change projections. *Nature Geoscience*, *7*(10), 703–708.
Sigmond, M., & Scinocca, J. F. (2010). The influence of the basic state on the northern hemisphere circulation response to climate change. *Journal of Climate*, *23*(6), 1434–1446. https://doi.org/10.1175/2009JCLI3167.1
Sigmond, M., & Shepherd, T. G. (2014). Compensation between resolved wave driving and parameterized orographic gravity wave driving of the Brewer-Dobson circulation and its response to climate change. *Journal of Climate*, *27*(14), 5601–5610. https://doi.org/10.1175/JCLI-D-13-00644.1
Smith, A. K. (2003). The origin of stationary planetary waves in the upper mesosphere. *Journal of the Atmospheric Sciences*, *60*(24), 3033–3041. Retrieved from https://journals.ametsoc.org/view/journals/atsc/60/24/1520-0469_2003_060_3033_toospw_2.0.co_2.xml
Virtanen, P., Gommers, R., Oliphant, T. E., Haberland, M., Reddy, T., Cournapeau, D., et al. (2020). SciPy 1.0: Fundamental algorithms for scientific computing in Python. *Nature Methods*, *17*, 261–272. https://doi.org/10.1038/s41592-019-0686-2

Waskom, M., Botvinnik, O., drewokane Hobson, P., David Halchenko, Y., Lukauskas, S., Lee, A., et al. (2016). *seaborn: v0.7.1*. https://doi.org/10.5281/zenodo.54844

White, R. H., Battisti, D. S., & Sheshadri, A. (2018). Orography and the Boreal Winter Stratosphere: The importance of the Mongolian Mountains. *Geophysical Research Letters*, *45*(4), 2088–2096. https://doi.org/10.1002/2018GL077098

Yiğit, E., & Medvedev, A. S. (2016). Role of gravity waves in vertical coupling during sudden stratospheric warmings. *Geoscience Letters*, *3*(1), 27.